# Optofluidic Fabry-Pérot sensor for water solutions at high flow rates

**Gediminas Gervinskas,**[1] **Daniel J. Day,**[1] **and Saulius Juodkazis**[1,2,*]

[1]*Centre for Micro-Photonics, Faculty of Engineering and Industrial Sciences, Swinburne University of Technology, Hawthorn, VIC, 3122, Australia*
[2]*Melbourne Centre for Nanofabrication, 151 Wellington Road, Clayton, VIC 3168, Australia*
[*]*SJuodkazis@swin.edu.au*

**Abstract:** Optofluidic sensor for water solutions has been fabricated using a transfer adhesive film and simple all-room-temperature procedures. Performance of a Fabry-Perot (FP) cavity subjected to the high water throughput of $\sim$ 2 ml per 1 min (at a 0.8 m/s flow velocity) was spectrally characterized. The 25-$\mu$m-wide cavity can be repeatedly subjected to pressures causing up to a 1.5% its width's increase upon pressure cycling. Potential of the new optofluidic platform for applications where (i) large water volumes should be filtered as well as (ii) for measurements of turbulence onset in two-dimensional flows at high 1 m/s velocity are discussed. We show possibility to use FP cavity for the pressure sensing at sensitivity of $\Delta\lambda/\Delta P \simeq 0.075$ nm/Pa and for the refractive index sensing at $\Delta\lambda/\Delta n \simeq 390$ nm per the refractive index unit.



**OCIS codes:** (120.2230) Fabry-Pérot; (120.5475) Pressure measurement; (310.6845) Thin film devices and applications.

## References and links

1. A. Isha, N. Yusof, M. Ahmad, D. Suhendra, W. Yunus, and Z. Zainal, "A chemical sensor for trace V (V) ion determination based on fatty hydroxamic acid immobilized in polymethylmethacrylate," Sens. Actuators B **114** (1), 344–349 (2006).
2. J. Wu and M. Gu, "Microfluidic sensing: state of the art fabrication and detection techniques," J. Biomed. Opt. **16**(8), 080901 (2011).
3. K. Xiao and D. G. Grier, "Sorting colloidal particles into multiple channels with optical forces: Prismatic optical fractionation," Phys. Rev. E **82**(5), 051407 (2011).
4. H. Misawa and S. Juodkazis, "Photophysics and photochemistry of a laser manipulated microparticle," Prog. Polym. Sci. **24**, 665–697 (1999).
5. M. Miwa, S. Juodkazis, and H. Misawa, "Drag of laser trapped micro-particle," Jpn. J. Appl. Phys. **39**(4A), 1930–1933 (2000).
6. E. Brasselet and S. Juodkazis, "Optical angular manipulation of liquid crystal droplets in laser tweezers," J. Nonlinear Opt. Phys. Mater. **18**(2), 167–194 (2009).
7. L. Y. Yeo and J. R. Friend, "Ultrafast microfluidics using surface acoustic waves," Biomicrofluidics **3**, 012002 (2009).
8. D. Y. C. Chan, R. R. Dagastine, and L. R. White, "Forces between a rigid probe particle and a liquid interface - I. The repulsive case," J. Colloid Interface Sci. **236**, 141–154 (2001).
9. N. Wu, Y. Zhu, S. Brown, J. Oakeshott, T. S. Peat, R. Surjadi, C. Easton, P. W. Leech, and B. A. Sexton, "A pmma microfluidic droplet platform for in vitroprotein expression using crude E. coli S30 extract," Lab Chip **9**, 3391–3398 (2009).
10. G. Gervinskas, D. Day, and S. Juodkazis, "High-precision interferometric monitoring of polymer swelling using a simple optofluidic sensor," Sens. Actuators B **159**(1), 39–43 (2011).
11. I. R. Young, S. Zieger, and A. V. Babanin, "Global trends in wind speed and wave height," Science **332**(6028), 451–455 (2011).

#160597 - $15.00 USD Received 10 Jan 2012; revised 6 Feb 2012; accepted 6 Feb 2012; published 16 Feb 2012

12. H. Xia, D. Byrne, G. Falkovich, and M. Shats, "Upscale energy transfer in thick turbulent fluid layers," Nat. Phys. **7**(4), 321–324 (2011).
13. D. Lange, C. Storment, C. Conley, and G. Kovacs, "A microfluidic shadow imaging system for the study of the nematode caenorhabditis elegans in space," Sens. Actuators B **107**(2), 904–914 (2005).
14. Z. Wu, N. Nguyen, and X. Huang, "Nonlinear diffusive mixing in microchannels: theory and experiments," J. Micromech. Microeng. **14**, 604–611 (2004).
15. S. Wang, Z. Jiao, X. Huang, C. Yang, and N. Nguyen, "Acoustically induced bubbles in a microfluidic channel for mixing enhancement," Microfluid. Nanofluid. **6**(6), 847–852 (2009).
16. H. Kido, M. Micic, D. Smith, J. Zoval, J. Norton, and M. Madou, "A novel, compact disk-like centrifugal microfluidics system for cell lysis and sample homogenization," Colloids Surf. B **58**(1), 44–51 (2007).
17. J. Wu, D. Day, and M. Gu, "Polymeric optofluidic Fabry-Pérot sensor by direct laser machining and hot embossing," Appl. Opt. **50**(13), 1843–1849 (2011).
18. H. Shao, D. Kumar, S. Feld, and K. Lear, "Fabrication of a Fabry–Pérot cavity in a microfluidic channel using thermocompressive gold bonding of glass substrates," J. Microelectromech. Syst. **14**(4), 756–762 (2005).
19. W. Chen, K. Shull, T. Papatheodorou, D. Styrkas, and J. Keddie, "Equilibrium swelling of hydrophilic polyacrylates in humid environments," Macromolecules **32**(1), 136–144 (1999).
20. S. Igarashi, A. Itakura, M. Toda, M. Kitajima, L. Chu, A. Chifen, R. Forch, and R. Berger, "Swelling signals of polymer films measured by a combination of micromechanical cantilever sensor and surface plasmon resonance spectroscopy," Sens. Actuators B **117**(1), 43–49 (2006).
21. P. Tabeling, *Introduction to Microfluidics* (Oxford University Press, 2005).
22. Y. Zel'dovich and Y. P. Raizer, *Physics of Shock Waves and High-Temperature Hydrodynamic Phenomena* (Dover, 2002).
23. A. Vailionis, E. G. Gamaly, V. Mizeikis, W. Yang, A. Rode, and S. Juodkazis, "Evidence of super-dense Aluminum synthesized by ultra-fast micro-explosion," Nat. Commun. **2**, 445 (2011).
24. S. Juodkazis, H. Misawa, E. G. Gamaly, B. Luther-Davis, L. Hallo, P. Nicolai, and V. Tikhonchuk, "Is the nano-explosion really microscopic?," J. Non.-Cryst. Solids **355**(18-21), 1160–1162 (2009).

## 1. Introduction

Inexpensive and high-throughput microfluidic sensors are required for monitoring water pollution, detection of contaminants of molecular, viral, and bacterial nature [1]. For certification of drinking water, it is necessary to test large 100 ml volumes, which are usually too large to handle by a microfluidic chip. By combining up to ten channels with identical sensing capabilities it is possible to reduce volume per channel and time of measurements. Hence, a 10 ml volume is a target for the filtered volume in a single channel. This would require flow rates of $\sim 2.5$ m/s for a typical 2-mm-wide and 25-$\mu$m-deep microchannel with a built in Fabry-Pérot (FP) sensing area. For a high spectral selectivity, the depth of the FP chamber has to be 20-30 $\mu$m for spectral shifts on the order of 1 nm at the visible wavelengths to be reliably detected at a high video-rate temporal resolution. Narrow channels and high flow rates are also required for micro-particle detection, counting and sorting applications, and nano-/micro rheology research [2–9].

We have recently demonstrated a simple optofluidic sensor with a FP cavity using thermal embossing in PMMA [10] where FP-mirrors were separated by 25 $\mu$m. However, the semi-transparent FP mirrors required for the spectral measurements in transmission were found to be solvent permeable. Seeping of water into the PMMA substrates was the fastest among the tested solvents: ethanol, methanol, and water. In order to use such sensors for analysis of large volumes of water they should be optimized for a lower solvent permeability, still be inexpensive (under a 1$/chip as in the earlier design [10]), and should handle flows at high $\sim 1$ m/s rates, which are close (or enter) the laminar-to-turbulent flow regime for two dimensional (2D) flows [11, 12].

Microfluidic channels using a double-sided adhesive tape [13] for a simple straight [14, 15] and more complex channels [16] have been reported; however, this method never been used for the more demanding interferometric FP cavity definition in optofluidics.

Here, we demonstrate a sensor design all made at room conditions using a transfer adhesive film (TA) which defined a 25-$\mu$m-deep micro-channel suitable for spectrally sensitive FP detection. Such sensor is faster to make, it has a non-permeable bottom glass plate, and lesser

#160597 - $15.00 USD Received 10 Jan 2012; revised 6 Feb 2012; accepted 6 Feb 2012; published 16 Feb 2012

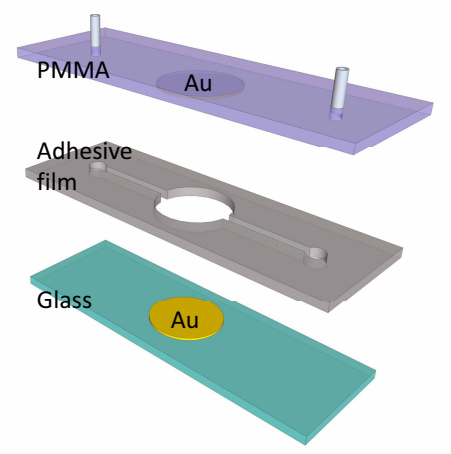


Fig. 1. Parts of optofluidic sensor: the bottom plate was glass, the channel profile was cut out of a transfer adhesive film (ARclad 8026, Adhesives Research Inc.) by a $CO_2$-cutter, and the top plate was PMMA. Gold mirrors were $\sim$ 40-nm-thick.

spectral drift due to PMMA swelling (only the top mirror is water permeable). We show, that highly sensitive measurements of $\sim 0.1-1$ nm/s spectral shifts can be detected and changes of refractive index of solution by $\Delta n \simeq 1\times10^{-2}$ ($\Delta\lambda/\Delta n \simeq 390$ nm/RIU, RIU is the refractive index unit) in the channel can be reliably detected using monitoring of the FP-fringe shifts at a video-rate. We show a new application of an optofluidic FP cavity as a pressure sensor with sensitivity $\Delta\lambda/\Delta P \simeq 0.075$ nm/Pa.

## 2. Experimental

Thermally evaporated gold mirrors of FP cavity were 40-nm-thick. The finesse of the FP in air was 2.5-2.6, slightly higher as those defined by embossing of Kapton [10].

The fabricated microfluidic chip was connected to a peristaltic pump (Minipuls 3, Gilson) to flow water through the micro-channel. The average flow velocity was directly measured by collecting water from the exit tube during a fixed time $\sim 1$ min with the $10^{-3}$ g precision scales and was proportional to the speed of rotation (measured in rotations per minute [rpm]) of the peristaltic pump.

Spectrometric measurements were carried out using the same setup as reported earlier [10]. White light was focused into a spot of $\sim 1$ mm on the central part of the FP mirror, collected into a fiber-coupled portable spectrometer (QE65000, Ocean Optics) at 0.4 nm spectral resolution and monitored over tens of minutes to few hours.

## 3. Results

### *3.1. Fabrication: interferometric chip using an adhesive film*

One of the time consuming steps in fabrication of microfluidic PMMA sensors is thermal embossing and bonding [17, 18]. In the case of FP-cavities, the flatness over the mirror regions is of the key importance for a reproducible spectral detection of spectral shifts of a fringe pattern; the shifts are due to changes on the channel width, which can be caused by: (i) adhesion of the analyte to the mirror surfaces, (ii) a permeability of the thin FP-mirrors as we reported recently [10], (iii) a change of refraction index of solution, or (iv) due to presence of micro-

#160597 - $15.00 USD Received 10 Jan 2012; revised 6 Feb 2012; accepted 6 Feb 2012; published 16 Feb 2012

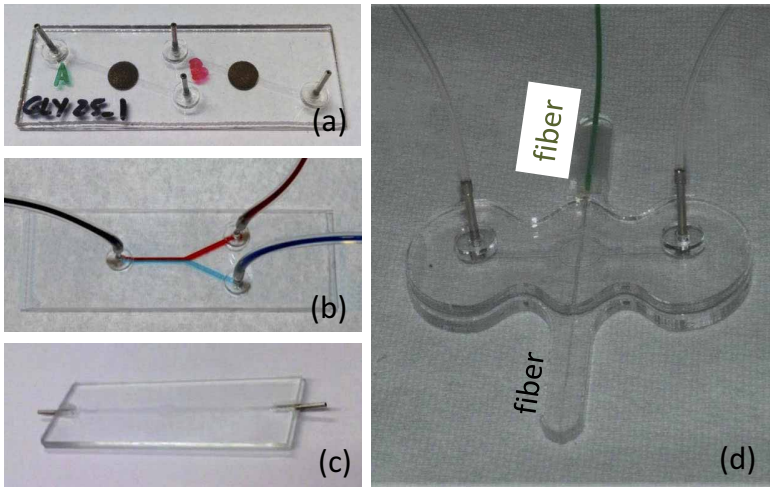


Fig. 2. Adhesive film-based designs for micro-fluidic chip fabrication. Realization of different optofluidic designs all using the principle shown in Fig. 1: (a) realization of two channels in one chip ("A" and "B"; this design is used for the refractive index and pressure sensing measurements), (b) fluid selector, (c) flat chip for reduction of the back-pressure in high-flow chip and (d) fiber-in-a-channel at cross-aligned geometry. Food dyes are used in the selector shown in (b), at the equal pressures in both shoulders; by changing relative pressure in the channels one or the other dye/solution can be delivered.

particles inside the channel.

Here, we demonstrate a method to define the depth of the FP-chamber and channel (Fig. 1) by use of a transfer adhesive (ARclad 8026 Adhesives Research Inc.) and manual pressure (for $\sim$ 10 s) to glue together the plates. ARclad 8026 is a silicone-based 25 $\mu$m-thick TA tape, which is UV and moisture resistant. Channel pattern was cut in TA by $CO_2$ laser (VLS 2.30, Versa Laser) without carbonization. The laser output power to cut TA without carbonization was 5 mW. Diameter of the laser beam was $\sim$ 100 $\mu$m. Channel is formed by a single pass along a circumference of the designed channel pattern.

The TA is water impermeable and has a good mechanical durability. It is advantageous to use TA as compared with thermal embossing due to several reasons: (i) it shortened time of chip fabrication by 2-3 times, as there are fewer production steps, (ii) adhesive has a selected uniform thickness, hence, a better reproducibility between samples was achieved, and (iii) different chip geometries can be realized. Flexibility of the new design is demonstrated by making a prototype chips shown in Fig. 2: an insertion of the single mode fiber into a channel at an 90 deg angle (d), making a flow selector (b) or a flat-chip (c). In the case of the fiber and flat-chip, thermal embossing was not required as the channel was formed in TA and fiber insertion groove is pre-fabricated in the top PMMA plate (note, fiber can be inserted after the chip is fabricated). All the experiments of refractive index and pressure sensing were carried out in a chip made by the sequence shown in Fig. 1 and shown in Fig. 2(a).

Using glass for the bottom plate of a chip provides advantage of having a flat mirror surface, greater mechanical stability of a whole system and impermeability to water. The top-plate of the chip made of PMMA allows a simple and strong attachment of inlet/outlet connections and different geometries, e.g., planar tube alignment is amendable and can be used to introduce optical fibers or operate at very high flow rates.

#160597 - $15.00 USD Received 10 Jan 2012; revised 6 Feb 2012; accepted 6 Feb 2012; published 16 Feb 2012

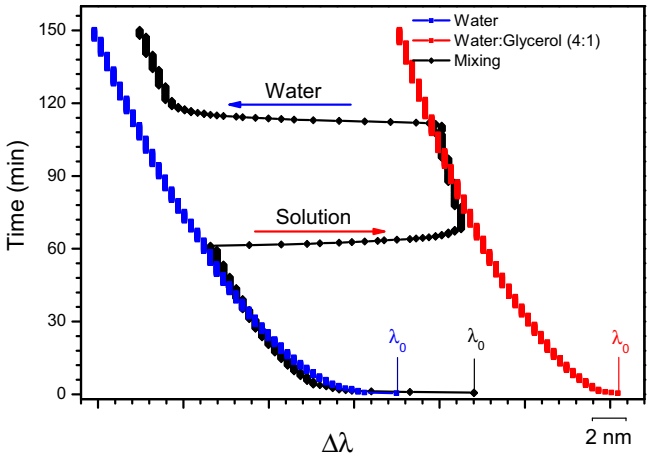


Fig. 3. Transients of spectral peak shifts in the case of different solutions and switching between them. The refractive index of water and the 4:1 mixture with glycerol were $n_w = 1.333$ and $n_{g25\%} = 1.364$, respectively, at wavelengths $\sim 650$ nm. Arrows show switching between water and glycerol solutions. The $\lambda_0$ is the starting position of the FP peak; a horizontal offset was used for clarity. Three measurements were carried out in separate identically prepared chips. Spot size of the beam used in spectral measurements of transmission was $\sim 1$ mm. Measurements were carried out after filling the channels without flow or when liquids were exchanged the flow rate was 0.04 m/s. Spectral sampling rate: one point per 15 s. Finesse of the FP cavity $F = 2.6$.

### *3.2. Refractive index and pressure sensing*

Figure 3 shows transients of the selected peaks of FP-fringes at $\lambda_0 \simeq 650$ nm in three identically fabricated channels; a minor difference between the mirrors was caused by a slight distance change from an evaporation target. The water permeation through the mirror into PMMA top plate is causing the spectral drift as shown in (Fig. 3) and was reported earlier [10]. Slower permeation rate and PMMA swelling (narrowing of the FP-cavity) was observed for the water-glycerol mixtures as would be expected due to larger glycerol molecules. The rate of permeation was approximately half of that observed in chips where both plates were out of PMMA for the same thickness of Au-mirrors [10]. It is noteworthy, that polymer swelling itself can be used as a sensing principle [19, 20].

Changes of the refractive index inside the channel were detected by switching from water to the water-glycerol mixture; the corresponding refractive index change is $\Delta n = 3.1 \times 10^{-2}$. Sensitivity of the refractive index sensing is $\Delta\lambda/\Delta n \simeq 390$ nm/RIU. The white light illumination spot on the FP-mirror was $d \simeq 1$ mm and determined the switching time limit as $t_s = d/v = 1$ ms to 1 s for the flow speeds of $v = 1$ m/s and 0.1 cm/s, respectively. The actual switching time was about 1 s in our experiments as defined by a manual switch of channels in the peristaltic pump. The width of the channel was approximately 1 mm and similar speed of selection between two solutions can be achieved using an auxiliary selector shown in Fig. 2(b).

The actual switching time between two solutions was traced with sensitivity $\sim$5 nm/min at the used spectral sampling speed of the one measurement per 15 s for the 2.5 h experiment shown in Fig. 3. The rate of pressure change of $\sim 1$ nm/s was observed when the fastest 0.38 m/s flow was turned on and off (Fig. 4(b)).

Figure 4 shows measurements in the same channel and demonstrates the repeated on-off

#160597 - $15.00 USD Received 10 Jan 2012; revised 6 Feb 2012; accepted 6 Feb 2012; published 16 Feb 2012

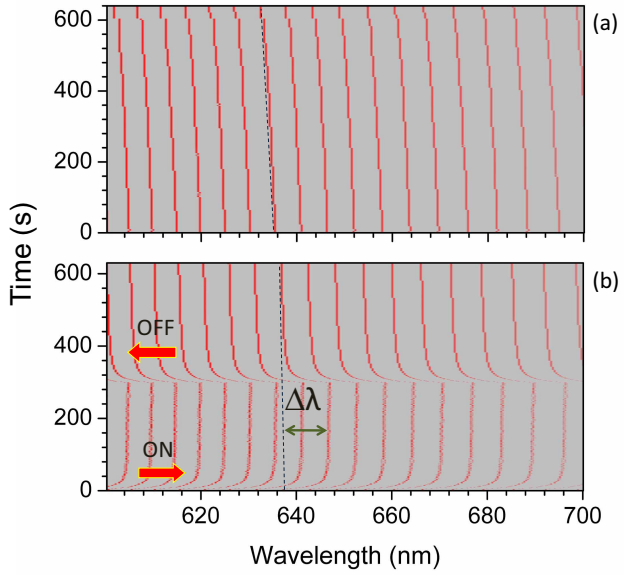


Fig. 4. Spectral shifts of the FP-fringes over time by switching ON/OFF peristaltic pump. The pump rotation speeds are: (a) 0.1 and (b) 10 rpm; corresponding to: 0.38 cm/s and 0.38 m/s flow velocity. The pump switching ON-OFF transients are marked; dashed-lines are eye guides for the peak tracking. Spectral sampling rate: point per 1 s (a) and 5 points per 1 s (b).

switching performance of the FP-cavity and summarizes monitoring of spectral shifts of the FP fringes at different flow rates and the on-off switching transients. Narrowing of the FP cavity (due to a PMMA swelling) at the lowest flow rate was changed to an expansion at the larger speeds. Even at the highest flow rates of $v \simeq 1$ m/s the adhesive was holding the plates well and after the pump was switched off, the FP fringes followed the standard slow flow behavior (see, extended regions in Figs. 4(a) and 4(b)). The on-off switching at the highest flow rates of $v \simeq 1$ m/s (limited by a tube's detachment from the channel) was achieved without degradation of the FP cavity nor channel. Adhesion of a TA film to the top and bottom plates remain uncompromised (without recognizable leaks and delamination) after up to 6 hours of testing. During one hour stress-testing of a structural integrity of a microfluidic channel water is pumped at the maximum speed ($v \simeq 1$ m/s) and pump makes $\sim 24000$ "On" and "Off" cycles (similar testing is shown in Fig. 4). The only reason of channel degradation was swelling of the top PMMA plate as we reported earlier and for the water solutions occurred after prolonged several hours of operation [10]. These optofluidic chips are intended for the fast measurements which are shorter than 5-10 min.

The pressure changes in the channel can be measured by monitoring spectral shifts of the FP cavity (see, Fig. 4). To quantify the pressure change, $\Delta P$, we, first, measured the vertical height of a spraying solution from a nozzle and, then, velocity is calculated from the balance of kinetic and potential energies. At the fixed flow rate, the velocity of solution in the tube of arbitrary diameter is calculated from Bernoulli equation (the diameter of the syringe tube used as nozzle is known):

$$P_1 + \rho g h_1 + \frac{1}{2}\rho v_1^2 = P_2 + \rho g h_2 + \frac{1}{2}\rho v_2^2 \qquad (1)$$

#160597 - $15.00 USD Received 10 Jan 2012; revised 6 Feb 2012; accepted 6 Feb 2012; published 16 Feb 2012

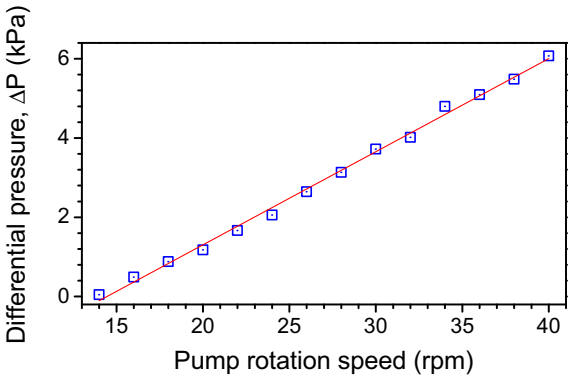


Fig. 5. Experimental measurements of a differential pressure, $\Delta P$, created by the peristaltic pump at different pump rotation speeds. Line is the linear fit.

where $P_1$ and $P_2$ are pressures in the pump and in atmosphere (101325 Pa), respectively; $\rho$ is the density of water, $g = 9.8$ m/s$^2$ is the Earth's gravity constant, $h_1$, $h_2$ equals zero as both nozzle and pump are at the same ground level, $v_1$ is the speed of liquid in the pump, whereas $v_2$ is the speed of liquid exiting the nozzle.

Figure 5 shows results of the differential pressure, $\Delta P$, calculations vs rotation speed of the peristaltic pump. At the pumping speed of 10 rpm, the pressure estimate was $\Delta P \sim 160$ Pa. The shift of peak position in experimentally observed spectrum ($\Delta\lambda$) was $\sim$12 nm (at the wavelengths around $\sim$785 nm). This defines a sensitivity of device $\Delta\lambda/\Delta P \simeq 0.075$ nm/Pa. As the spectral resolution of our portable spectrometer is only 0.4 nm, we can reliably detect change of $\Delta P \simeq 5.33$ Pa in the channel.

The spectral shifts of FP fringes can be used as a flow meter over the dynamic range of 100 as shown in Fig. 4. The flow velocity, $v$, of liquid whose viscosity is, $\mu$, driven by the pressure difference, $\Delta P$, scales with the transverse dimensions of channel, $b$, and its length, $L$ as [21]: $v \propto \frac{b^2}{\mu L}\Delta P$.

The FP cavity build in a microfluidic channel is acting as a pressure or flow velocity sensor. Shift of the fringes over approximately the free spectral range $\Delta\lambda \simeq 10$ nm corresponds to the FP cavity change by $\sim \lambda/2 \simeq 325$ nm, i.e., an increase by 1.3% as was observed in the case of 0.14 m/s.

## 4. Discussion

The peak positions of FP fringes undergo small erratic shifts as flow rate increases (see, Fig. 4(b)). It is related to the pump's noise whose rotation speed is known (e.g., 10 rpm for 0.38 m/s flow velocity). Fourier analysis (not shown) revealed that spectral shifts of FP fringes are related to the rotation speed of the pump and is the main source of the noise in spectral measurements. Syringe pumps would be preferable for measurements at increased signal-to-noise ratio.

Data analysis of Figs. 3 and 4 shows that changing of refractive index or flow rate in the channel can be monitored by spectral shifts of the FP fringe pattern. The presence of a slow PMMA swelling in water can be easily accounted for as a baseline shift (it can be slightly different from channel to channel). This shows that 10 ml per 5 min at a 1 m/s flow velocity is a feasible target for filtration in a simple channel held together by an adhesive spacer, which

#160597 - $15.00 USD Received 10 Jan 2012; revised 6 Feb 2012; accepted 6 Feb 2012; published 16 Feb 2012

defines the channel geometry.

The presented simple channels can be operated at flow rates corresponding to the Reynolds number (Re) $Re \equiv \frac{\rho v x}{\mu} > 2300$, where $v$ is the velocity of flow and $x$ is the characteristic linear dimension of the flow. The Reynolds number represents the ratio of the inertia to viscous force and predicts onset of turbulency of a 3D flow when $Re > 2300$. The optofluidic channels can be used for a little explored turbulence onset phenomena in 2D flows in an easy and accessible way, e.g., using selector of two colored fluids (see, Fig. 2(b)).

The 2D flows are important due to their relevance in geo-physical, atmospheric, oceanography and fundamental hydrodynamics fields of research [11, 12]. The fundamental down scaling laws of hydrodynamics [22] justifies the use of micro-fluidic chip to model 2D turbid phenomenon relevant to formation of cyclones and warm/cold oceanic flows which all have *width/depth*$\simeq 10^2 - 10^3$ ratio as in a microfluidic chip 2 mm/20 $\mu$m = 100. We recently demonstrated that hydrodynamic scaling allows to compare laser induced material mass flow induced by micro-explosions [23] with their macro counterparts which have energies $10^{21}$ times higher and the space and time scales increased by $10^7$ [24].

## 5. Conclusions

We demonstrate a simplified and versatile optofluidic platform where the channel is made in the adhesive film which is also used to assemble and hold the top and bottom plates of FP cavity. The channel was tested at high pressure corresponding to flow velocity up to 1 m/s and is capable for transport of comparatively large (10 ml) volumes in a reasonable operation time (5 min) required for actual certified drinking water tests. FP cavity of 25 $\mu$m width was reliably withstanding a high flow rate (high pressure) load during spectral measurements with a detection noise mainly caused by an uneven pressure of the peristaltic pump.

## Acknowledgments

We are grateful to Prof. A. Babanin for discussions on the 2D flows and turbulence threshold and to Adhesives Research Inc. which kindly provided the adhesive tape for prototyping the optofluidic chip.

#160597 - $15.00 USD Received 10 Jan 2012; revised 6 Feb 2012; accepted 6 Feb 2012; published 16 Feb 2012